Solar Energy Materials & Solar Cells 122 (2014) 88–93

Contents lists available at ScienceDirect

Solar Energy Materials & Solar Cells

journal homepage: www.elsevier.com/locate/solmat

Assessing the origin of the S-shaped *I–V* curve in organic solar cells: An improved equivalent circuit model

Lijian Zuo [a,b], Jizhong Yao [a,b], Hanying Li [a,b,*], Hongzheng Chen [a,b,*]

[a] State Key Laboratory of Silicon Materials, Zhejiang University, Hangzhou, 310027 PR China
[b] MOE Key Laboratory of Macromolecular Synthesis and Functionalization, Department of Polymer Science and Engineering, Zhejiang University, Hangzhou 310027, PR China

ARTICLE INFO

Article history:
Received 2 August 2013
Received in revised form
3 November 2013
Accepted 11 November 2013
Available online 8 December 2013

Keywords:
Organic solar cells
Kink
S shape curve
Equivalent circuit model
Simulation

ABSTRACT

Formation of S-shaped *I–V* curve or the so-called kink has been shown detrimental to organic solar cells (OSC) performance. Previous researches have indicated that a variety of reasons could count for the origin of the S-shaped *I–V* curve. However, its origin is still not clear. In this contribution, we investigated the origin of S-shaped *I–V* curve from the view of an equivalent circuit model (ECM) in OSCs. The proposed ECM involves a rectifying junction connected with a donor/accepter (D/A) junction in series. OSCs with and without a Schottky barrier that was a rectifying junction were fabricated to verify the modeled results. And the good reproduction of experimental results confirmed the validity of our model. The results indicate that the origin of S-shaped *I–V* curve in OSCs is associated with the rectifying junction. With this model, the effects of the rectifying junction on the shape of *I–V* characteristic and its effect on device parameters are analyzed: fill factor (FF) dropped, short circuit current density decreased, open circuit voltage however, remained. Also, from simulation, we varied the parameters of the rectifying junction to study their influence on the device performance.

1. Introduction

Organic solar cells (OSCs) have shown great potential to provide clean and renewable energy due to their low cost, lightweight, flexibility and environment friendly merits [1–5]. Recently, device performance has improved rapidly, with literature reported efficiency up to 10% [6–9], lifetime around thousands of hours [10–12], and energy payback time within 1 day [13,14]. Although these encouraging improvements promise OSCs a bright future, still further improvements are required to bring this technique into practical application. Usually, the device performance is limited by poor absorption, low charge carrier mobility and short exciton diffusion length [15–18]. Besides, the fundamental understanding of device physics is also required for the further improvement in device performance of OSCs.

As a matter of fact, abnormal current–voltage (*I–V*) curves of OSCs would be induced due to degradation by moisture or oxygen [19,20], inferiority of materials or fabrication procedures [21], and other unexpected factors [22]. One of the most frequent failure modes of OSCs that appeared in literatures is the formation of S-shaped *I–V* curve [19]. With the appearance of the S-shaped *I–V* curve, the fill factor (FF) is significantly ruined. As such, formation of an S-shaped *I–V* curve is detrimental to device performance. And fundamental knowledge of the S-shape and the strategies to remove it are essentially important for the practical application of organic solar cells in the future [23,24]. Most recently, several groups have investigated the origins of the S-shaped *I–V* curves from the view of charge transportation, accumulation and recombination by solving the Poisson equation, current continuity equations, and current equations including both drift and diffusion [25–29]. By changing the device structures, controlled S-shaped *I–V* curves were formed and these results indicated that the S-shaped *I–V* curve could be induced by different reasons: interfacial dipole, charge accumulation at interface, unbalanced charge transportation, and electrode/active layer interfacial Schottky barriers. Although the S-shaped *I–V* curves might originate due to different reasons, the shapes of *I–V* curves are nearly identical, indicating that some common physical basis could account for the formation of S-shaped *I–V* curves: bias-voltage-dependent photocurrent recombination.

An equivalent circuit model helps in understanding the work principles of OSCs, interpreting the *I–V* characteristics and device performances, and optimizing the performance of OSCs, through a quantitative simulation. The conventional circuit model was developed in the context of inorganic solar cells and had been adopted to interpret the performance of OSCs as well [30]. Furthermore, due to the complex working mechanisms of OSCs,

* Corresponding authors at: Department of Polymer Science and Engineering, Zhejiang University, Hangzhou 310027, PR China. Tel.: +86 571 87952557; fax: +86 571 87953733.
E-mail addresses: hanying_li@zju.edu.cn (H. Li), hzchen@zju.edu.cn (H. Chen).

0927-0248/$ - see front matter © 2013 Elsevier B.V. All rights reserved.
http://dx.doi.org/10.1016/j.solmat.2013.11.018

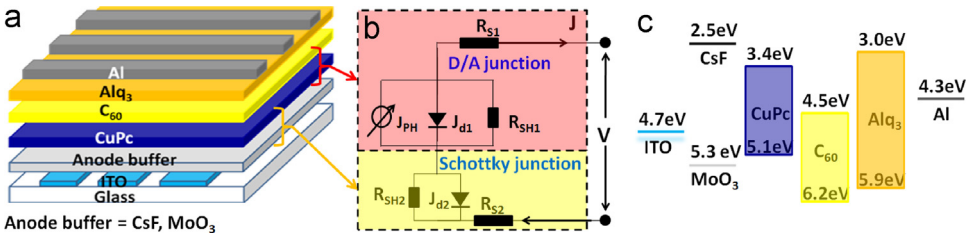

Fig. 1. (a) Schematic diagram for the device structure, (b) improved circuit model: red part is the traditional equivalent circuit model for the D/A junction and the yellow part is the equivalent circuit model for the Schottky junction, and (c) schematic diagram of energy level of each layer in the solar cell. The CuPc:C_{60}/Alq3/Al part in (a) contributed to the diode 1 (red part in (b)), in which J_{ph} is photocurrent formed at the CuPc/C_{60} interface, J_{d1} represents the charge recombination at the CuPc/C_{60} interface, R_{s1} stands for the series resistance contributed by the resistance of each layer and interfacial resistance, and R_{sh1} is induced by the direct contact of electrode with CuPc layer (during the thermal evaporation process, thermal diffusion of hot Al atom would permeate into the active layers. This could be suppressed through insertion of Alq_3) or traps in active layers. And the CuPc/CsF/ITO part contributes to the Schottky junction (yellow part), in which J_{d2} represents the leakage current at CuPc/CsF interface, and R_{s2} stands for the series resistance of each layer and interface resistance. And R_{sh2} is contributed by the direct contact of CuPc and ITO. (For interpretation of the references to color in this figure legend, the reader is referred to the web version of this article.)

the models need to be modified to better simulate the complicated *I–V* characteristics [31,32,33]. For example, Balderrama et al. proposed a model with an additional diode connected with a D/A junction in parallel to interpret the surface recombination or current leakage due to the unfavorable contacts of donor/cathode or acceptor/anode [33]. With the improved models, where all different physics processes could be simulated by the electric elements, the influence of certain parameter on OSCs' performance becomes clear and predictable. However, none of these models could be used to well interpret the origin of the S-shaped *I–V* curves.

In view of the previous studies, an improved equivalent circuit is proposed to interpret the origin of S-shaped *I–V* curve and its effect on device performance. We found that most of the S-shaped *I–V* curves could be simulated by the equivalent circuit model featuring a D/A junction connected with a rectifying junction in series (shown in Fig. 1), which we argued was the origin of the S shape curve. In order to confirm this model, we fabricated planar heterojunction (PHJ) solar cells with different anode buffer layers (molybdenum trioxide (MoO_3) and cesium fluoride (CsF)). The device structures (ITO/buffer layer/CuPc/C_{60}/Alq_3/Al) and schematic diagram of energy levels for each layer are shown in Fig. 1. Due to work function difference of MoO_3 and CsF (5.3 eV and 2.5 eV, respectively [34,35]), different contacts were formed: with MoO_3 as anode buffer, Ohmic contact was formed; however, with CsF, Schottky barrier was formed, which would induce rectifying properties at anode interface. Our simulated *I–V* curves fit well with the experimental data, which confirms the validity of the improved equivalent circuit model. Finally, we argue that the existence of a rectifying junction and a D/A junction connected in series is the essential reason for the formation of S shape curve.

2. Material and methods

2.1. Materials

All the materials were from Sigma Aldrich Corp., and used as received.

2.2. Device fabrication and characterization

Organic solar cells (device structure shown in Fig. 1) were fabricated as follows: first, ITO coated glass (150 nm, 8 Ω/□, *or Ω per square*) substrates were cleaned by detergent, de-ionized water, isopropanol, acetone, and ethanol in ultrasonic bath sequentially. After drying by N_2 gas flow, these substrates were placed in a vacuum chamber. The anode buffer layers (CsF and MoO_3) were deposited onto the substrates through vacuum thermal evaporation (VTE) at the base pressure of 4×10^{-4} Pa. CuPc (30 nm), C_{60} (60 nm), Alq_3 (5 nm), and Al (100 nm) were also deposited by the VTE method in the same chamber as well. Current–voltage (*I–V*) characteristics were recorded on a Keithley 236 measurement source unit, in dark and under 1 sun (100 mW/cm^2) AM 1.5G simulated solar illumination (Abet) of our solar cells. And the light intensity was calibrated by a standard silicon diode. The device area was 9 mm^2. All the procedures were performed in ambient air.

3. Theory

Typically, OSCs are composed of a donor and acceptor junction (D/A junction), similar to conventional silicon p–n junction cells [36]. The equivalent circuit model is shown in the red part of Fig. 1 (b), and the corresponding equation is presented below:

$$J = R_{sh}/(R_s+R_{sh})\{J_0[\exp(qV/nk_BT - qAJR_s/nk_BT)-1]+V/R_{sh}\}-J_{sc} \quad (1)$$

where J is the current density through the whole device, V is the bias voltage, J_0 is the leakage current density, q is the charge unit, n is the ideal factor, k_B is the Boltzmann constant, T is the temperature in Kelvin, A is the device area, R_s is the series resistance, R_{sh} is the parallel resistance, and J_{SC} is the short circuit current density of the device. The first term on the right side of the equation is the exponential diode current, the second term is the leakage current through the shunt resistance and the last is the photon-induced current.

In the improved equivalent circuit model, we utilize a rectifying junction element connected with the D/A junction in series to interpret the bias-voltage-dependent carrier recombination. We apply exponential diode current (Eq. (2a)) to describe the D/A junction inside the OSC, and another diode (Eq. (2b)) to indicate the rectifying properties induced by Schottky barrier, interfacial dipole, unbalanced charge transport, etc. The basic working principles in the improved equivalent circuit model are that the current densities through the D/A junction and the Schottky junction are identical (Eq. (2d)) and the bias voltage is shared by the two junctions (Eq. (2c)). This relation is numerically illustrated by the following equations:

$$J_1 = R_{sh1}/(R_{s1}+R_{sh1})\{J_{01}[\exp(qV_1/nk_BT - qAJ_1R_{s1}/nk_BT)-1]+V_1/R_{sh1}\}-J_{sc} \quad (2a)$$

$$J_2 = R_{sh2}/(R_{s2}+R_{sh2})\{J_{02}[\exp(qV_2/nk_BT - qAJ_2R_{s2}/nk_BT)-1]+V_2/R_{sh2}\} \quad (2b)$$

$$V_1+V_2 = V \quad (2c)$$

$$J_1 = J_2 = J \tag{2d}$$

To confirm the validity of the equivalent model, we purposely introduced a Schottky junction at anode interface of ITO/anode buffer layer/CuPc/C_{60}/Alq_3/Al PHJ solar cells (shown in Fig. 1a). The Schottky junction was controlled by the work function of the buffer layer (MoO_3 or CsF). In the case of CsF as anode interfacial layer, the work function of CsF modified ITO (2.5 eV) is much lower than the HOMO of CuPc (5.1 eV). Due to the energy level alignment and the mismatched energy level of CsF and CuPc, space charge depletion region forms. Thus, Schottky junction at the interface of ITO/CsF and CuPc is expected. In contrast, in the case of MoO_3, whose work function (5.3 eV) is close to the HOMO of CuPc (5.1 eV), the interfacial Schottky junction is negligible.

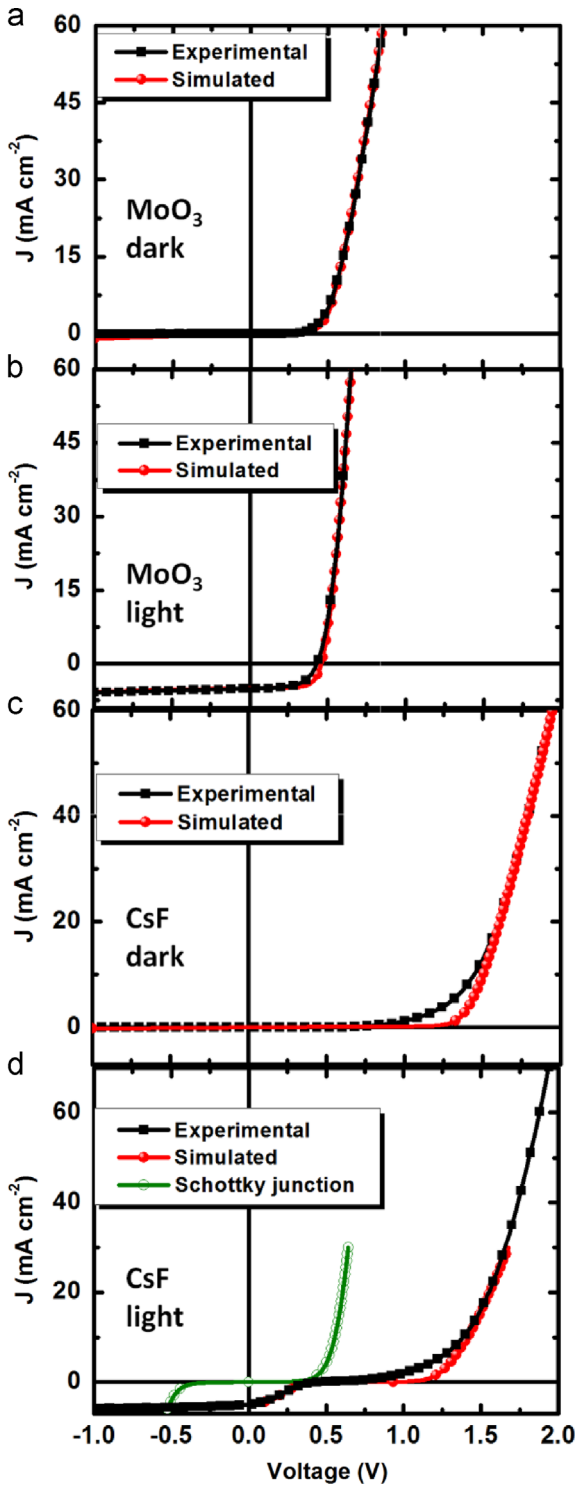

Fig. 2. Experimental and simulated *I–V* curves of devices with MoO_3 as anode buffer layer (a) in dark and (b) under illumination (AM 1.5G, 100 mW/cm^2), and with CsF as anode buffer layer (c) in dark and (d) under illumination.

4. Results and discussions

Fig. 2 shows the simulated and experimental *I–V* curve characteristics under AM 1.5 illumination and in dark for devices with MoO_3 or CsF as anode buffer layer. The fitting model gives quantitative calculations of the cell parameters, including R_s, R_{sh}, n and J_0 for both the ideal solar cell D/A junction and Schottky junction and all these parameters are summarized in Table 1. The modeling results fit the experimental data well along the whole voltage range. The good reproducibility verifies the validity of the model mentioned above. With the improved equivalent circuit, the origin of abnormal S shape *I–V* curve and its effects on the device performance were clearly interpreted.

4.1. *I–V* characteristics under illumination

Under illumination, we observe an S-shaped *I–V* curve for the cell of CsF but not for that of MoO_3. This difference can be explained by the existence of a Schottky junction in the CsF cell. When the bias reaches V_{OC} of the D/A junction, where the drift current is identical to the diffusion current, there is no net current in the whole device and all the bias is applied to the D/A junction to suppress the photocurrent. Thus, the existence of Schottky junction does not influence V_{OC}, because V_{OC} is generic nature of the D/A junction. As a result, in both cells (CsF and MoO_3), the values of V_{OC} are very close. This conclusion is consistent with other literature reports [37]. Near this region, the differential series resistance of D/A junction is very small (equal to the series resistance of D/A junction). But the differential resistance of the Schottky junction is large, which is equivalent to the differential resistance at 0 V bias for an individual Schottky junction (equivalent to the shunt resistance of the Schottky junction). Since the two junctions are connected in series, the current density is determined by the one with larger differential resistance. As a result, near V_{OC}, the Schottky junction dominates the *I–V* characteristics and the shape of *I–V* curve resembles that of the individual Schottky junction near its zero bias (Fig. 2d). This is essentially the reason for the formation of S-shaped *I–V* curve. Thus, we could safely conclude that any non-Ohmic contact or any rectifying junction connected with D/A junction in series would induce an S-shaped *I–V* curve. When the bias voltage further increases, the turn-on voltage has to drive both the D/A junction and the Schottky junction open in order to drive the whole device open, which is the reason for the increased turn-on voltage and the shift of the *I–V* curve toward higher voltage compared with those of the individual D/A junction (Fig. 2b and d).

At the forward bias smaller than V_{OC}, the photocurrent dominates the whole device, and thus the Schottky junction is reversely driven and becomes an obstacle to the charge collection, which caused significant carriers recombination at the anodes and subsequently ruined the FF. From the *I–V* curve of single Schottky junction (Fig. 2d), the photocurrent recombination represented by the Schottky junction was expected to be bias-voltage-dependent. With the bias voltage increasing, the photo-current density decreases and the obstacle to charge collection created by the Schottky junction decreases, too. As shown in Fig. 2, this bias-voltage-dependent recombination severely ruins the FF.

Table 1
Device parameters for both simulated *I–V* curve and the experimental *I–V* curve.

Anode interfacial layer	Experimental results				Simulated results			
	J_{SC}	V_{OC}	η[a]	FF[b]	R_s	R_{sh}	J_0	n
	mA/cm^2	V	%	/	Ω cm^2	kΩ cm^2	A/cm^2	/
MoO_3	5.2	0.42	1.35	0.63	4.5[c]	10[c]	7.0E−8[c]	1.2[c]
	5.0	0.44	0.60	0.28				
CsF	D:A junction				R_{s1}	R_{sh1}	J_{01}	n_1
					6.3[d]	10[d]	6.5E−9[d]	1.58[d]
	Schottky junction				R_{s2}	R_{sh2}	J_{02}	n_2
					0.05[d]	2[d]	1.5E−3[d]	2[d]

The device is characterized under AM 1.5G, 100 mW/cm^2. Device parameters are extracted from the *I–V* curve in dark. And the device area: 0.09 cm^2.

[a] OSC device efficiency.
[b] Fill factor.
[c] These parameters were obtained through fitting the MoO_3 based device *I–V* curve using Eq. (1).
[d] These parameters were obtained by fitting the CsF based device *I–V* curve using Eq. (2).

At the zero bias (the bias voltage is 0 V), the photo-generated current has to drive the Schottky junction before being collected at the electrode. That is equivalent to a "forward voltage" applied to the D/A junction. Thus the actual J_{SC} of the whole device is smaller than the photo-generated current density of D/A junction. And with reverse bias voltage increasing further, there would be a reverse compensate voltage, at which the photocurrent of the whole device is equal to the photocurrent of D/A junction. These equivalent "forward voltage" and "reverse compensate voltage" are expected to be determined by the work function of the buffer layer. The MoO_3 anode buffer layer with its larger work function provides a smaller "forward voltage" and, thus, higher measured J_{SC} compared to the case of CsF (Table 1).

4.2. *I–V* characteristics in dark

In dark, in the case of reverse bias, the bias voltage is shared by the two junctions and the total current density passing each of the junctions should be identical. Thus, the reverse current density is determined by the junction with smaller reverse current density at the same bias. On the other hand, at forward bias, the bias is shared by the D/A junction and the Schottky junction and the current density is also limited by the junction with smaller forward current density. The series resistance is theoretically the summation of the two junctions and the bias voltage has to reach the voltage at which both junctions are turned on to drive the series connected diode. In the case of CsF, the Schottky junction leads to a high turn on voltage (around 1.2 V). In contrast, the MoO_3 cell has a negligible Schottky junction so that the turn on voltage is much smaller (Fig. 2a and c).

Based on this model, we vary parameters of Schottky junction separately to check their influences on the *I–V* curve of the whole device. Fig. 3 shows *I–V* curves as a function of parameters of Schottky junction. In this modeling, we fix all the values fitted from the equivalent circuit model and vary the values separately to see their effects on the whole cell performance. It could be observed that the dark saturation current I_0, ideal factor n, and the shunt resistance R_{sh} dominate the threshold voltage of the Schottky junction. As n increases or I_0 decreases, the threshold voltage increases as well. The changes in the "kink" region of the S-shaped *I–V* curve are very sensitive to the shunt resistance R_{sh}. As shown in Fig. 1, R_{sh} is parallel connected to the Schottky junction; when R_{sh} is large, the Schottky junction dominates the charge collection. As R_{sh} becomes smaller, carriers would be easily collected through the smaller R_{sh} instead of the Schottky junction. As a result, bias-voltage-dependent charge recombination is suppressed. R_s has a strong effect on the slope of the *I–V* curve. The increasing R_s leads to a gradually decreased slope in the *I–V* curve. Thus, in order to achieve high efficient solar cells, the Schottky junction should be eliminated completely by increasing the leakage current or reducing the shunt resistance of the Schottky junction.

Thus, in order to eliminate the S-shaped *I–V* curve, one should 1) reduce the Schottky barrier at the interface, by utilizing an interfacial layer with proper energy level matching those of both active layer and electrode, and 2) increase the conductivity of interfacial layer (or reduce R_{sh2} or R_s in Fig. 1). In our case, the formation of S-shaped *I–V* curve could be suppressed by using an interfacial layer with higher work function (or deeper HOMO) (MoO_3, PEDOT:PSS). And higher conductivity (e.g. thinner thickness of PEIE [39] and PFN [9] layers, or highly doped layers such as Cs doped TiO_2 [40] and Cs doped ZnO [41]) is also an alternative way to remove the S-shaped *I–V* curve. In addition, our model refers the origin of S-shaped curve regarding the degradation of organic solar cells [38]. The degradation of interfacial materials (Ca or PEDOT:PSS) caused large resistance and mismatched work function with the bulk heterojunction active layer through, e.g., oxidation of Ca, and morphology change in PEDOT:PSS in air. The high series resistance and mismatched work function would block the charge collection at the electrode, leading to rectifying behavior and S-shaped *I–V* curve. This might be the physical origin of S-shaped *I–V* curve during degradation. This behavior could be interpreted as a rectifying junction connected with D/A junction in series, which is in consistence with our proposed improved equivalent circuit model.

And it should be noted that this model is not limited to Schottky barrier. Any junction with rectifying properties or non-Ohmic contact would induce the S-shaped *I–V* curve. However, this model is not adaptable for the case when significant leakage current of the device is induced. For example, in bulk heterojunction (BHJ) solar cells, both donor and acceptor are connected with the low work function anode interfacial layer. And significant leakage current would be induced at the acceptor/low work function anode interface and the formation of large leakage current should significantly decrease V_{OC}, according to the equation:

$$V_{OC} \propto \ln(J_{SC}/J_d) \tag{3}$$

where J_{SC} is the photocurrent and J_d is the leakage current [25]. Another limitation of this model is that there should be no photocurrent generation in the Schottky junction [42], which would compensate the D/A photocurrent and cause significant change in V_{OC}.

5. Conclusions

In conclusion, we assessed the essential reason for the S-shaped *I–V* curves by establishing an improved equivalent circuit model.

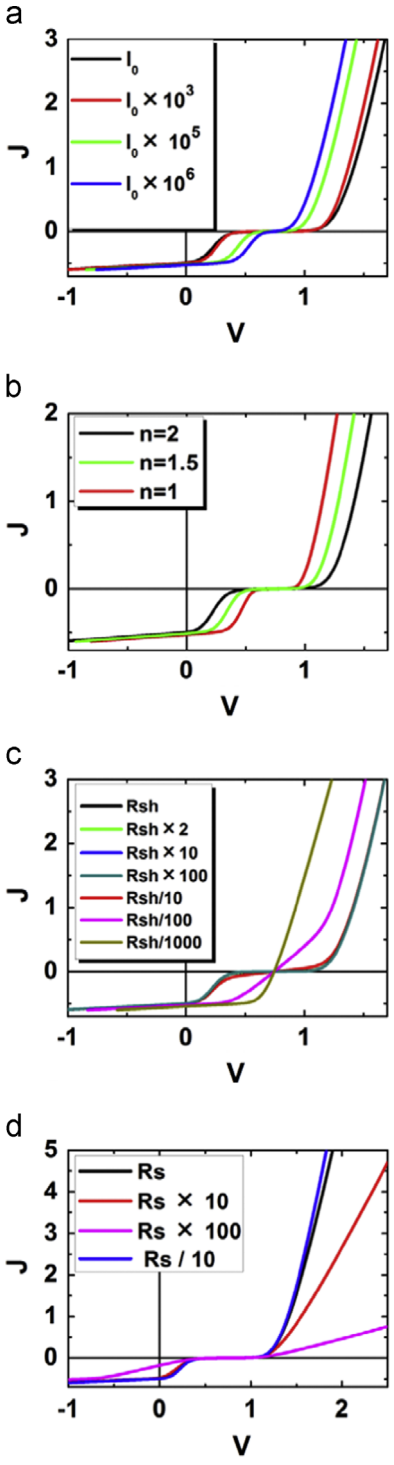

Fig. 3. Modeled *I–V* curves for CsF as the buffer layer with different (a) I_0, (b) n, (c) R_{sh}, and (d) R_s.

In the improved model, we proposed a rectifying junction element which is connected with the D/A junction in series, to interpret the bias-voltage-dependent photo-induced carrier recombination. The validity was confirmed by good reproduction of our experimental results. With the equivalent circuit model, effects of S-shaped *I–V* curve formation on the device performance were analyzed: formation of the *I–V* curve should have no influence on V_{OC}, but would ruin the FF and J_{SC}. The effect of variation in the Schottky junction on the whole device was also discussed. This work has implications for understanding the working mechanisms as well as optimizing device fabrication of OSCs.

Acknowledgment

This work was supported by the National Natural Science Foundation of China (Grants 50990063, 51261130582, 91233114, and 51222302), the Major State Basic Research Development Program (2014CB643503), Zhejiang Province Natural Science Foundation (Grant LZ13E030002), the Scientific Research Foundation for the Returned Overseas Chinese Scholars, State Education Ministry, and Fundamental Research Funds for the Central Universities (2012QNA4025).

References

[1] T.D. Nielsen, C. Cruickshank, S. Foged, J. Thorsen, F.C. Krebs, Business, market and intellectual property analysis of polymer solar cells, Sol. Energy Mater. Sol. Cells 94 (2010) 1553–1571.
[2] Z. He, C. Zhong, X. Huang, W.Y. Wong, H. Wu, L. Chen, S. Su, Y. Cao, Simultaneous enhancement of open-circuit voltage, short-circuit current density, and fill factor in polymer solar cells, Adv. Mater. 23 (2011) 4636–4643.
[3] Y. Sun, G.C. Welch, W.L. Leong, C.J. Takacs, G.C. Bazan, A.J. Heeger, Solution-processed small-molecule solar cells with 6.7% efficiency, Nat. Mater. 11 (2012) 44–48.
[4] G.J. Zhao, Y.J. He, Y.F. Li, 6.5% efficiency of polymer solar cells based on poly(3-hexylthiophene) and indene-C(60) bisadduct by device optimization, Adv. Mater. 22 (2010) 4355–4358.
[5] J. Yang, R. Zhu, Z. Hong, Y. He, A. Kumar, Y. Li, Y. Yang, A robust inter-connecting layer for achieving high performance tandem polymer solar cells, Adv. Mater. 23 (2011) 3465–3470.
[6] X. Li, W.C.H. Choy, L. Huo, F. Xie, W.E.I. Sha, B. Ding, X. Guo, Y. Li, J. Hou, J. You, Y. Yang, Dual plasmonic nanostructures for high performance inverted organic solar cells, Adv. Mater. 24 (2012) 3046–3052.
[7] J. You, L. Dou, K. Yoshimura, T. Kato, K. Ohya, T. Moriarty, K. Emery, C.-C. Chen, J. Gao, G. Li, Y. Yang, A polymer tandem solar cell with 10.6% power conversion efficiency, Nat. Commun. 4 (2013) 1446-1–1446-10.
[8] J. You, C.C. Chen, Z. Hong, K. Yoshimura, K. Ohya, R. Xu, S. Ye, J. Gao, G. Li, Y. Yang, 10.2% power conversion efficiency polymer tandem solar cells consisting of two identical sub-cells, Adv. Mater. (2013).
[9] Z. He, C. Zhong, S. Su, M. Xu, H. Wu, Y. Cao, Enhanced power-conversion efficiency in polymer solar cells using an inverted device structure, Nat. Photonics 6 (2012) 591–595.
[10] M. Jørgensen, K. Norrman, S.A. Gevorgyan, T. Tromholt, B. Andreasen, F.C. Krebs, Stability of polymer solar cells, Adv. Mater. 24 (2012) 580–612.
[11] F.C. Krebs, S.A. Gevorgyan, J. Alstrup, A roll-to-roll process to flexible polymer solar cells: model studies, manufacture and operational stability studies, J. Mater. Chem. 19 (2009) 5442–5451.
[12] M. Jørgensen, K. Norrman, F.C. Krebs, Stability/degradation of polymer solar cells, Sol. Energy Mater. Sol. Cells 92 (2008) 686–714.
[13] N. Espinosa, M. Hosel, D. Angmo, F.C. Krebs, Solar cells with one-day energy payback for the factories of the future, Energy Environ. Sci. 5 (2012) 5117–5132.
[14] N. Espinosa, R. Garcia-Valverde, F.C. Krebs, Life-cycle analysis of product integrated polymer solar cells, Energy Environ. Sci. 4 (2011) 1547–1557.
[15] T. Kirchartz, K. Taretto, U. Rau, Efficiency limits of organic bulk heterojunction solar cells, J. Phys. Chem. C 113 (2009) 17958–17966.
[16] Y. Shirota, H. Kageyama, Charge carrier transporting molecular materials and their applications in devices, Chem. Rev. 107 (2007) 953–1010.
[17] T.M. Clarke, J.R. Durrant, Charge photogeneration in organic solar cells, Chem. Rev. 110 (2010) 6736–6767.
[18] N. Banerji, S. Cowan, M. Leclerc, E. Vauthey, A.J. Heeger, Exciton formation, relaxation, and decay in PCDTBT, J. Am. Chem. Soc. 132 (2010) 17459–17470.
[19] F.C. Krebs, K. Norrman, Analysis of the failure mechanism for a stable organic photovoltaic during 10 000 h of testing, Prog. Photovolt. Res. Appl. 15 (2007) 697–712.
[20] K. Norrman, S.A. Gevorgyan, F.C. Krebs, Water-induced degradation of polymer solar cells studied by $H_2{}^{18}O$ labeling, ACS Appl. Mater. Interfaces 1 (2008) 102–112.
[21] L. Zuo, X. Jiang, L. Yang, M. Xu, Y. Nan, Q. Yan, H.Z. Chen, Sb_2O_3 anode buffer induced morphology improvement in small molecule organic solar cells, Appl. Phys. Lett. 99 (2011) 183306-1–183306-3.
[22] X.L. Hu, M.M. Shi, J. Chen, L.J. Zuo, L. Fu, Y.J. Liu, H.Z. Chen, Synthesis and photovoltaic properties of ester group functionalized polythiophene derivatives, Macromol. Rapid Commun. 32 (2011) 506–511.
[23] M.R. Lilliedal, A.J. Medford, M.V. Madsen, K. Norrman, F.C. Krebs, The effect of post-processing treatments on inflection points in current–voltage curves of roll-to-roll processed polymer photovoltaics, Sol. Energy Mater. Sol. Cells 94 (2010) 2018–2031.
[24] J. Alstrup, M. Jørgensen, A.J. Medford, F.C. Krebs, Ultra fast and parsimonious materials screening for polymer solar cells using differentially pumped slot-die coating, ACS Appl. Mater. Interfaces 2 (2010) 2819–2827.

[25] W. Tress, K. Leo, M. Riede, Influence of hole-transport layers and donor materials on open-circuit voltage and shape of *I–V* curves of organic solar cells, Adv. Funct. Mater. 21 (2011) 2140–2149.
[26] J.C. Wang, X.C. Ren, S.Q. Shi, C.W. Leung, P.K.L. Chan, Charge accumulation induced S-shape *J–V* curves in bilayer heterojunction organic solar cells, Org. Electron. 12 (2011) 880–885.
[27] A. Wagenpfahl, D. Rauh, M. Binder, C. Deibel, V. Dyakonov, S-shaped current–voltage characteristics of organic solar devices, Phys. Rev. B 82 (2010) 115306-1–115306-8.
[28] A. Kumar, S. Sista, Y. Yang, Dipole induced anomalous S-shape *I–V* curves in polymer solar cells, J. Appl. Phys. 105 (2009) 094512-1–094512-6.
[29] W. Tress, A. Petrich, M. Hummert, M. Hein, K. Leo, M. Riede, Imbalanced mobilities causing S-shaped *IV* curves in planar heterojunction organic solar cells, Appl. Phys. Lett. 98 (2011) 063301-1–063301-3.
[30] B. Mazhari, An improved solar cell circuit model for organic solar cells, Sol. Energy Mater. Sol. Cells 90 (2006) 1021–1033.
[31] A. Haldi, A. Sharma, W.J. Potscavage, B. Kippelen, Equivalent circuit model for organic single-layer diodes, J. Appl. Phys. 104 (2008) 064503-1–064503-3.
[32] A. Cheknanea, H.S. Hilalb, F. Djeffalc, B. Benyoucefd, J.P. Charlese, An equivalent circuit approach to organic solar cell modelling, Microelectron. J. 39 (2008) 1173–1180.
[33] V.S. Balderrama, M. Estrada, A. Cerdeira, B.S. Soto-Cruz, L.F. Marsal, J. Pallares, J. C. Nolasco, B. Iñiguez, E. Palomares, J. Albero, Influence of P3HT:PCBM blend preparation on the active layer morphology and cell degradation, Microelectron. Reliab. 51 (2011) 597–601.
[34] V. Shrotriya, G. Li, Y. Yao, C.-W. Chu, Y. Yang, Transition metal oxides as the buffer layer for polymer photovoltaic cells, Appl. Phys. Lett. 88 (2006) 073508-1–073508-3.
[35] M. Reinhard, J. Hanisch, Z.H. Zhang, E. Ahlswede, A. Colsmann, U. Lemmer, Inverted organic solar cells comprising a solution-processed cesium fluoride interlayer, Appl. Phys. Lett. 98 (2011) 053303-1–053303-3.
[36] J.A. Barker, C.M. Ramsdale, N.C. Greenham, Modeling the current–voltage characteristics of bilayer polymer photovoltaic devices, Phys. Rev. B 67 (2003) 075205-1–075205-9.
[37] C.M. Martin, V.M. Burlakov, H.E. Assender, D.A.R. Barkhouse, A numerical model for explaining the role of the interface morphology in composite solar cells, J. Appl. Phys. 102 (2007) 104506-1–104506-9.
[38] H. Jin, M. Tuomikoski, J. Hiltunen, P. Kopola, A. Maaninen, F. Pino, Polymer–electrode interfacial effect on photovoltaic performances in poly(3-hexylthiophene):phenyl-c61-butyric acid methyl ester based solar cells, J. Phys. Chem. C 113 (2009) 16807–16810.
[39] Y. Zhou, C. Fuentes-Hernandez, J. Shim, J. Meyer, A.J. Giordano, H. Li, P. Winget, Th. Papadopoulos, H. Cheun, J. Kim, M. Fenoll1, A. Dindar, W. Haske, E. Najafabadi, T.M. Khan, H. Sojoudi, S. Barlow, S. Graham, J.L. Brédas, S. R. Marder, A. Kahn, B. Kippelen, A universal method to produce low-work function electrodes for organic electronics, Science 336 (2012) 327–332.
[40] M.H. Park, J.H. Li, A. Kumar, G. Li1, Y. Yang, Doping of the metal oxide nanostructure and its influence in organic electronics, Adv. Funct. Mater. 19 (2009) 1241–1246.
[41] S. Kwon, K.G. Lim, M. Shim, H.C. Moon, J. Park, G. Jeon, J. Shin, K. Cho, T.W. Lee, J.K. Kim, Air-stable inverted structure of hybrid solar cells using a cesium-doped ZnO electron transport layer prepared by a sol–gel process, J. Mater. Chem. A 1 (2013) 11802–11808.
[42] S. Rajaputra, G. Sagi, V.P. Singh, Schottky diode solar cells on electrodeposited copper phthalocyanine films, Sol. Energy Mater. Sol. Cells 93 (2009) 60–64.